¹ Mohammad Zadehrostam Tarpouei

Improving the Efficiency of Solar Thermophotovoltaic Energy Conversion System



Abstract: - Solar energy can be directly or indirectly converted into other types of energy such as heat and electricity. However, several obstacles cause the insignificant use of such energy, including scientific and technical weaknesses in conversion due to lack of knowledge and field experiences, variable energy amount due to atmospheric and seasonal changes and radiation direction, as well as a very wide distribution scale. A comprehensive review of methods to improve the performance of solar thermophotovoltaic energy conversion systems in order to enhance efficiency is one of the most important aspects of innovation in this study. Computer modeling of thermal systems has various benefits, such as adjusting the cost of prototype construction, optimizing system components, estimating the amount of output energy, predicting system temperature changes, and other low-priority cases. This study also presents the results of the execution of the relevant files by engineering equation solver (EES) software ©1992-2003 S.A. Klein offers Commercial Version 6.883-3D (09/01/03). The results are represented in the form of tables and comparative plots. The investigations carried out include thermodynamic, exergetic, and economic parameters.

Keywords: efficiency, energy conversion system, exergetic, economic, solar thermophotovoltaic

I. INTRODUCTION

Thermophotovoltaic (TPV) is the process of directly converting heat into electricity through photons. A basic thermophotovoltaic system consists of a thermal emitter and a photovoltaic diode cell. The temperature of the thermal lever between different systems varies between about 900 and 1300 degrees Celsius. However, TPV devices can extract energy from any high-temperature emitter through a photovoltaic device forming a photothermal engine. The emitter may be a solid material or an engineered structure.

Srikhirin et al [1] presented a review of absorption refrigerant technology such as different models of ARSs, working fluids, and modification of absorption processes [2, 3]. Kececiler et al [4] conducted an experimental study on the thermodynamic analysis of a reversible ARS using a mixture of water and lithium bromide. Joudi and Lafta [5] presented a steady-state computer simulation model to predict the performance of a water-lithium bromide-based ARS.

P. Aguiar et al. (2002) introduced a reliable model of a solid oxide fuel cell with internal fuel modification [6]. Aguiar published valuable papers in 2004 [7] and 2005 [8] on the modeling of planner solid oxide fuel cells. The first paper introduced a stable and one-dimensional model of a planner solid oxide fuel cell with direct internal reforming and co-flow. P. Costamagna et al. (2004) presented an electrochemical model for a new planner solid oxide fuel cell as a bridge between tubular and planner geometries [9].

S.Campanari and P.Ior (2004) investigated the effect of changing the thickness of the cell components on the voltage drop of the solid oxide fuel cell [10]. The researchers proved that the performance of an anodic support cell was superior to that of an electrolytic support cell or a cathodic support cell [11, 12]. X.Xue et al. (2005) investigated the effects of mass transfer, heat transfer, and electrochemical equations on a tubular solid oxide fuel cell [13]. Yutong Qi published two papers on the dynamic modeling of solid oxide fuel cells in 2005 and 2006. In his first article, he investigated the effect of the penetration of reactants in porous layers [14]. In the second article, the dynamic effect of mass transfer and energy transfer on the performance of solid oxide fuel cells was evaluated [15]. One of the valuable studies in the field of solid oxide fuel cell modeling is H. Iwai et al. (2011) [16]. In this study, a model of a planner solid oxide fuel cell with internal fuel reforming and anode support was presented. Min Zeng et al. (2012) presented a three-dimensional model and investigated the effects of parameters such as diffusion coefficient, ambient temperature, and flow arrangement modes on battery performance [17].

The current research aims to investigate solar absorption cycles. First, the preliminary and thermal principles of conventional absorption systems and solar absorption systems are examined. According to the variable amount of solar radiation during different months and hours of the heat seasons, time-dependent thermal and thermodynamic analysis (dynamic analysis) is analyzed. Then, the complete arrangement of solar absorption systems in the form

¹Department of Mechanical Engineering, Islamic Azad **University**, Lahijan Branch, Lahijan, Iran

of exergetic problems and the second law are examined in such a way that the conditions for a comprehensive thermoeconomic analysis of the system and its optimization are provided.

II. RESEARCH METHODOLOGY

Thermoeconomic analysis of single-effect solar absorption refrigeration cycle

The necessary steps for thermoeconomic analysis of a system are 1) thermodynamic and exergetic analysis (calculation of E), 2) economic analysis (calculation of z), and 3) thermoeconomic analysis based on the above steps. In the previous section, we mentioned the thermodynamic analysis of the single-effect absorption cycle.

According to the components of the cycle as a general system, we can define the exergetic costing of all flows, the cost balance equation, and the auxiliary relations to solve the cost balance equations as follows:

Table (1) reflects the necessary equations for the thermoeconomic analysis of the system.

Table 1: Thermoeconomic relations for a water-lithium bromide single-effect absorption refrigeration cycle

Sub-system	Fuel	Product	Auxiliary relations
The solar component of the cycle	$\dot{C}_{FSolar} = c_{Hsolar} * Q_{aux}^{TOTAL}$	$\dot{C}_{FSolar} + \dot{Z}_{Solar}$	Q_{aux}^{TOTAL} $SEPTEMBER$ $= \sum_{MONTH=MAY} Q_{auxMONTH}$
Generator	$\dot{C}_F = \dot{C}_{PSolar}$	$\dot{C}_7 + \dot{C}_3 - \dot{C}_4$	$ \frac{\dot{C}_{7}}{\dot{m}_{7}(e_{7}-c_{3})} - \frac{(e_{4}-e_{7})\dot{C}_{1}}{\dot{m}_{7}(e_{7}-e_{3})(e_{4}-e_{3})} - \frac{\dot{C}_{4}}{\dot{m}_{4}(e_{4}-e_{3})} = 0 $
Absorbent	$\dot{C}_6 + \dot{C}_{10}$	Ċ ₁	$\frac{\dot{C}_6}{\dot{E}_6} = \frac{\dot{C}_{10}}{\dot{E}_{10}}$
Condenser	$\dot{\mathcal{C}}_1$	\dot{C}_2	
Evaporator	$\dot{C}_9 - \dot{C}_{10}$	$\dot{C}_{P,total}$	
Heat exchanger	$\dot{\mathcal{C}}_4 - \dot{\mathcal{C}}_5$	$\dot{C}_3 - \dot{C}_2$	$\dot{C}_4 - \left(\dot{E}_4 \middle/ \dot{E}_5\right) \dot{C}_5 = 0$
pump	$\dot{\mathcal{C}}_E$	$\dot{C}_1 - \dot{C}_2$	-
The whole system	$\dot{C}_H + \dot{C}_E$	$\dot{\mathcal{C}}_{P,total}$	-

This section describes how to configurator parameters and business information. As explained before, the single-effect absorption refrigeration cycle has 5 heat exchangers, 1 pump, and 2 expansion valves. According to the relations provided by Berhane H. [19], the initial and annual investment cost of the above equipment is determined as follows.

$$PEC_g = 516.612 * A_g + 268.45$$
 (1) $\dot{Z}_g = CRF * PEC_g$

where PEC_g is the initial capital cost and \dot{Z}_g is the annual capital cost of the generator in dollars. Considering the interest rate of 3.5% (i) and the number of cycle operations in 10 years, the investment return is calculated. Subsequently, the following relations can be used for other cycle absorption component equipment.

$$PEC_a = 516.612 * A_a + 268.45$$
 (2) $\dot{Z}_a = CRF * PEC_a$

$$PEC_{c} = 516.612 * A_{c} + 268.45$$

$$\dot{Z}_{c} = CRF * PEC_{c}$$

$$PEC_{e} = 516.612 * A_{e} + 268.45$$

$$\dot{Z}_{e} = CRF * PEC_{e}$$

$$PEC_{p} = 630 * W^{0.4}$$

$$\dot{Z}_{e} = CRF * PEC_{p}$$
(5)

where W is the amount of work consumed in the absorber pump, PEC_p is the initial capital cost and \dot{Z}_p is the annual capital cost of the absorber pump in dollars.

III. RESULTS

1. Proposed model for technical and economic analysis

The sample house model shown in Figure (1) provided by G.A. Florides et al. [19] is reviewed for analysis. By considering an insulated roof, insulated walls, double-glazed windows, internal awnings, and night ventilation in summer, the load on the house is reduced to a minimum. The above factors are considered economically sustainable. The double walls are made of 0.10 m hollow bricks and a 0.02 m plaster layer on each side. Also, an insulation layer of 0.05 m is embedded in the middle. The roof consists of 0.15 m of heavy concrete, 0.05 m of polystyrene insulation, 0.07 m of ingots, and 0.004 m of asphalt covered with 0.55 aluminum paint absorbing sunlight.

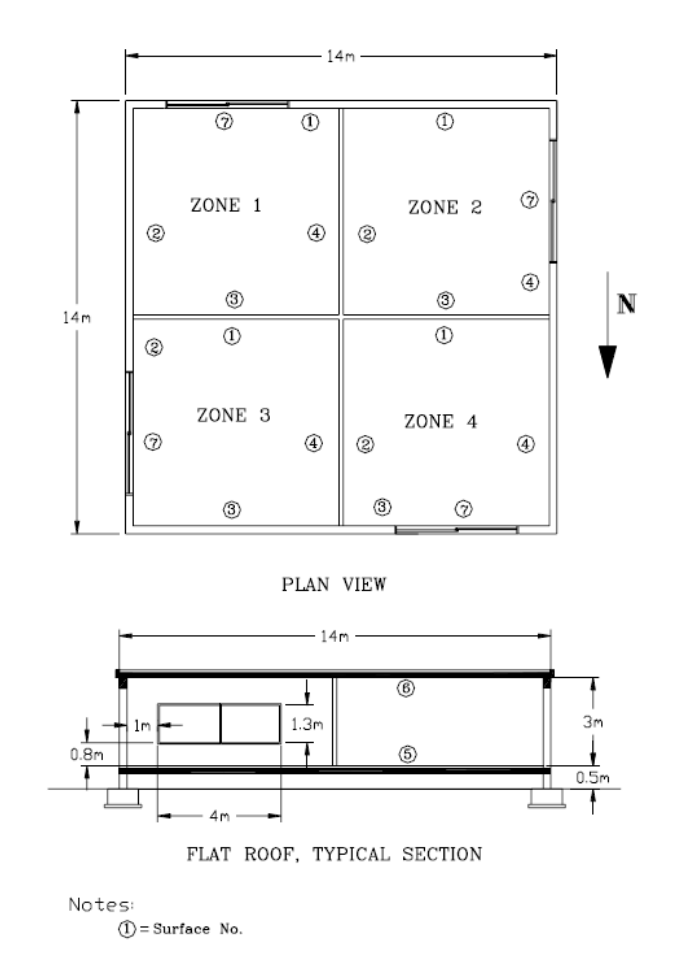


Figure 1: Plan of the house used for ventilation with a cooling load of 11kw

Basic modes for thermodynamic and exergetic analysis of the sample problem

The basic mode values and their types are represented in Table (2). According to the recommendation of Kızılkan et al.[20] and Misra's [21], we ignore the changes in the heat transfer coefficient of all single-effect solar absorption

cycle heat exchangers due to the low range of temperature changes of design variables related to temperature during the process optimization.

Table 2: basic values for thermodynamic and exergetic analysis of water-lithium bromide single-effect absorption cycle

Input variable for cycle analysis	Basic value
T ₁₁	90 °C
m_{11}	0. 197 $^{m{k}m{g}}/_{m{S}}$
$T_{13} = T_{15}$	25 . 5 °C
T ₁₄	35.8 °C
T ₁₆	34.3 °C
T ₁₇	16.5 °C
m_{17}	1.5 $^{oldsymbol{kg}}/_{oldsymbol{s}}$
Q_e	11 kw
$arepsilon_{ShX}$	0.64
$arepsilon_g$	0.61
$arepsilon_a$	0.45
$arepsilon_c$	0.62
$arepsilon_e$	0.3

Thermodynamic and exergetic results of the absorption component of the solar absorption cycle

After initialization and program execution, various parameters are realized at cycle points. Table (4) shows the capacity of heat exchangers, absorber pump, amount of fuel and product, and the ratio of exergetic destruction and exergetic efficiency of cycle components.

According to the results, the highest amount of exergy loss occurs in the condenser (kW 0.3425) with YDc 45% and the absorber (kW 0.2946) with YDa 26.74%. The reason is the high-temperature difference between the cooling water and the input and output flows to the condenser and absorber and high heat loss to the environment (high exergy loss). Also, due to the relatively high-temperature difference between the input flow from the generator and the output of the absorber pump, the exergetic efficiency of the heat recovery exchanger is low. Heat-dispersing equipment includes a condenser and absorber. The result of their operation is reflected in the form of thermal waste and exergy loss (0.44 kW). In general, the system shows low $\mathcal{E}_{\text{total}}$ value (21.62%) and high exergy loss (71.46% (1.102kW)).

Table 3: The thermodynamic and exergetic parameters resulting from cycle analysis in the basic mode

Points	Temperature	Pressure	Fluid mass	Chemical	Density	Entropy	Enthalpy	Exergy
	°C	(kPa)	rate	compound	LiBr	$\frac{kw}{kg^{\circ}C}$	(kW)	(kW)
			(kg/sec)		(%)	∕ κg ∪		
1	31.3	1.283	0.0299	water- lithium bromide	49.9	0.2193	63	0.06489
2	31.3	7.262	0.0299	water- lithium bromide	49.9	0.2193	63	0.06489
3	55.6	7.262	0.0299	water- lithium bromide	49.9	0.386	116.3	0.1719
4	81.9	7.262	0.0252	water- lithium bromide	59.2	0.4632	193.3	1.508

5	49.5	7.262	0.0252	water- lithium bromide	59.2	0.2791	130.2	1.3
6	48.4	1.283	0.0252	water- lithium bromide (Dual- phase)	59.2	0.2787	130.2	1.303
7	63.7	7.262	0.0047	Steam	0.0	8.171	2544.6	0.5286
8	39.7	7.262	0.0047	Water	0.0	0.5682	166.2	0.006579
9	10.7	1.283	0.0047	Water (Dual- phase)	0.0	0.5887	166.2	-0.02202
10	10.7	1.283	0.0047	Steam	0.0	8.883	2520.1	-0.5778
11	90.0	101.325	0.1970	Water	0.0	1.193	376.9	5.117
12	73.9	101.325	0.1970	Water	0.0	1.003	309.5	2.981
13	25.5	101.325	0.3058	Water	0.0	0.374	106.8	-0.01864
14	35.8	101.325	0.3058	Water	0.0	0.5158	149.9	0.226
15	25.5	101.325	0.3019	Water	0.0	0.374	106.8	-0.0184
16	34.3	101.325	0.3019	Water	0.0	0.4954	143.7	0.1612
17	16.5	101.325	1.5000	Water	0.0	0.246	69.2	0.6789
18	14.7	101.325	1.5000	Water	0.0	0.2206	61.9	1.036

Table 4: Useful exergetic characteristics resulting from cycle analysis in the base mode

Components	Fuel.ex	Prod.ex	Ex.dest	Ex.loss	Ex.D.ratio	Ex.L.ratio	Ex.eff
	E _F (kW)	$E_p(kW)$	$E_D(kW)$	E _{l.} (kW)	Y _D (%)	Y ₁ (%)	(%) ε
generator	2.136	1.9	0.2711	-	0.2001	-	87.31
absorbent	0.725	0.06	0.4155	0.2446	0.3066	55	8.95
condenser	0.5286	0.0066	0.3425	0.1796	0.2527	45	1.245
evaporator	0.5558	0.3569	0.1989	-	0.1468	-	64.21
heat exchanger	0.2085	0.107	0.1015	-	0.07492	-	51.32
The whole system	2.3045	0.3569	1.355	0.44	75.48	24.52	16.71

Time-dependent and dynamic simulation of solar absorption refrigeration cycle

Three types of collectors proposed by Ileri A [19] for solar absorption cycles in the Middle East are used in the simulation. The intersection angle in these collectors is considered 30 degrees. Due to the small range of collector level changes and collector temperature changes (due to the control conditions applied on the pump between the collector and the hot water storage tank), the change in the coefficient of heat loss of the collector has been omitted in the thermal and thermoeconomic analysis of solar collectors [23].

The results of the dynamic analysis of the system for 5 months of the year are reflected in Table (5). The temperature of the water tank and the inlet temperature of the collector during system start-up are the same as the ambient temperature. However, as the results show, the temperature of the tank at the beginning of the morning is around 65 degrees Celsius, which is also applied in the calculations. Changing the design parameters of the system such as the level of the collector and the volume of the hot water storage tank leads to a change in the temperature of the tank between 2 and 5 degrees Celsius. However, this has been neglected in the calculations. As the results show, the load of the auxiliary heater (Q_{aux}) at the end of the day, at night, and at the beginning of the morning is equal to the required heat in the generator due to the application of the control function at the low-temperature level of the system. In fact, the solar system is not effective in providing the required load of the generator, that is, the amount of FNP is equal to zero. However, as the day begins and the hours increase towards noon, the solar system works effectively. Around 14:00 in the afternoon, the solar system provides about 90% of the necessary thermal load of the generator.

Table 5: The results of the dynamic simulation of the system in the months of May, June, and July

Time	$T_{S,2}$	Q_{aux}	FNP	$T_{S,2}$	Q_{aux}	FNP	$T_{S,2}$	Q_{aux}	FNP
of day	(°C)	(Watt)	(%)	(°C)	(Watt)		(°C)	(Watt)	(%)
			May			June	July		
1	68.04	13018	0	68.1	13018	0	68.12	13018	0
2	67.82	13018	0	67.88	13018	0	67.9	13018	0
3	67.61	13018	0	67.67	13018	0	67.69	13018	0
4	67.4	13018	0	67.46	13018	0	67.48	13018	0
5	67.19	13018	0	67.25	13018	0	67.27	13018	0
6	66.98	13018	0	67.04	13018	0	67.06	13018	0
7	64.81	13018	0	64.81	13018	0	64.81	13018	0
8	67.08	13018	0	67.62	13018	0	67.73	13018	0
9	72.29	14545	0.1173	73.27	14102	0.083	73.69	14013	0.0764
10	77.44	10316	0.2076	78.36	9516	0.269	78.95	9179	0.2949
11	80.57	6133	0.5289	81.49	5389	0.586	82.21	4905	0.6232
12	82.2	3594	0.7239	83.11	2852	0.781	83.88	2266	0.826
13	82.15	2275	0.8253	83.06	1532	0.882	83.84	912.3	0.9299
14	80.71	2316	0.8221	81.6	1573	0.879	82.32	942.5	0.9276
15	77.83	3482	0.7325	78.67	2757	0.788	79.24	2176	0.8329
16	73.49	5819	0.553	74.31	5135	0.605	74.61	4677	0.6407
17	71.23	9338	0.2827	71.66	8672	0.333	71.82	8431	0.3524
18	70.06	11170	0.1419	70.28	10823	0.168	70.36	10698	0.1782
19	69.45	12125	0.0686	69.56	11944	0.082	69.6	11879	0.08751
20	69.13	13018	0	69.19	13018	0	69.21	13018	0
21	68.91	13018	0	68.97	13018	0	68.99	13018	0
22	68.69	13018	0	68.75	13018	0	68.77	13018	0
23	68.47	13018	0	68.53	13018	0	68.55	13018	0
24	68.25	13018	0	68.31	13018	0	68.33	13018	0

Figure (2) represents the amount of changes in the heat load consumed in the auxiliary heater during the day for different levels of the solar collector in May. The increase in the temperature of the tank in the noon hours is caused by the increase in the intensity of direct solar radiation to the surface of the collectors. As expected, the amount of thermal load consumed during these hours decreases.

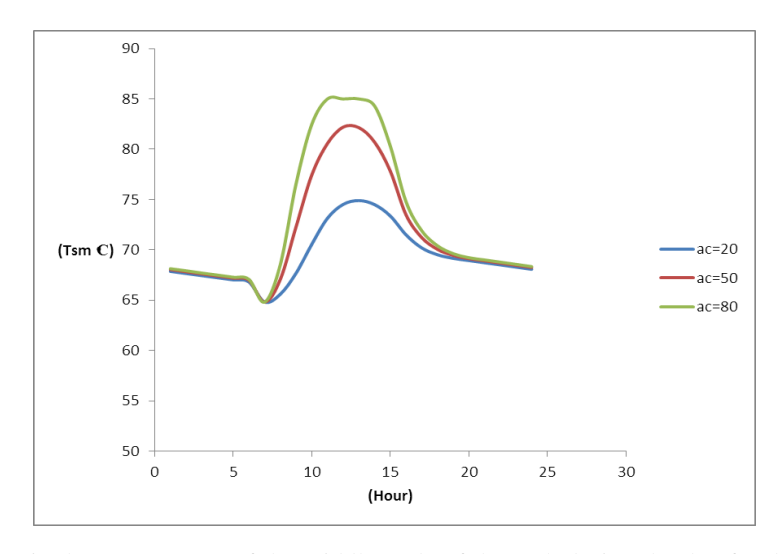


Figure 2: The change in the temperature of the middle node of the tank during the day for different levels of the solar collector in May with $W_{TANK} = 1500$ Kg, $T_{11} = 85^{\circ}C$

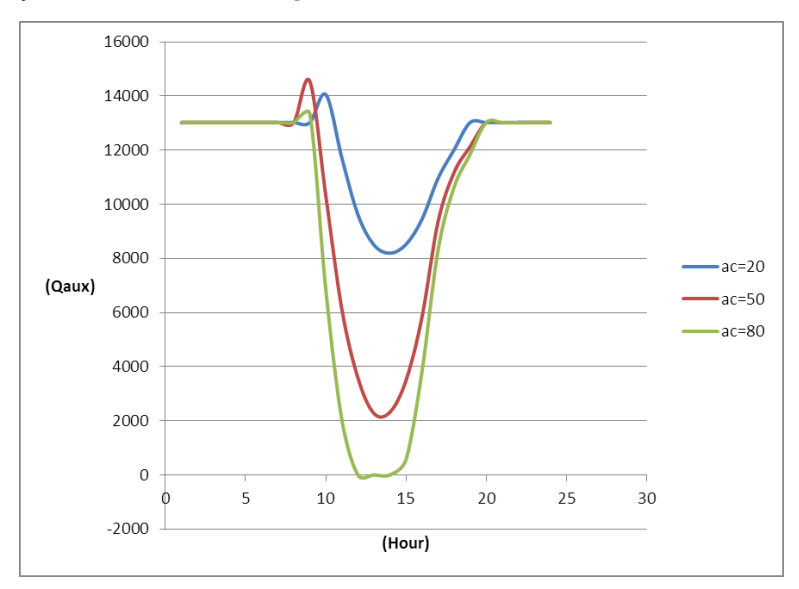


Figure 3: The change in heat load of the auxiliary heater during the day for different levels of the solar collector in May with $W_{TANK} = 1500$ Kg, $T_{11} = 85^{\circ}C$

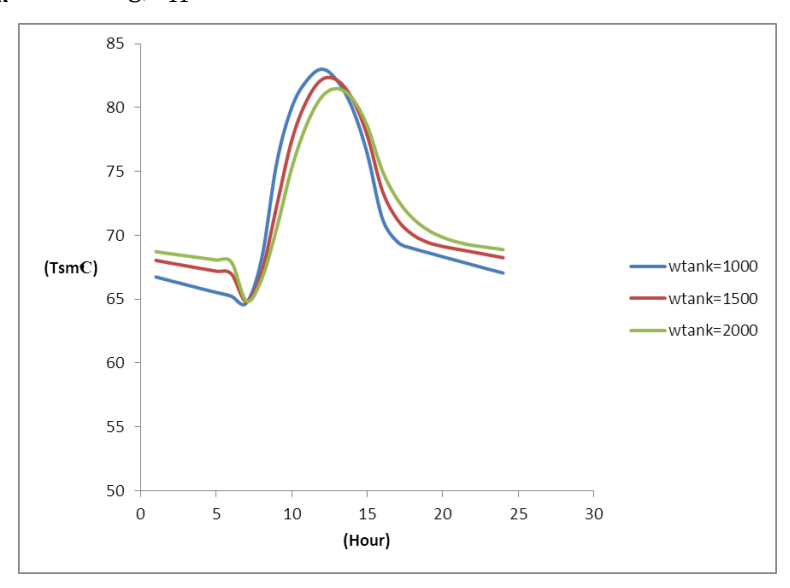


Figure 4: The temperature change of the middle node of the tank during the day for different levels of the solar collector in May with $A_C = 50m^2$, $T_{11} = 85^{\circ}C$

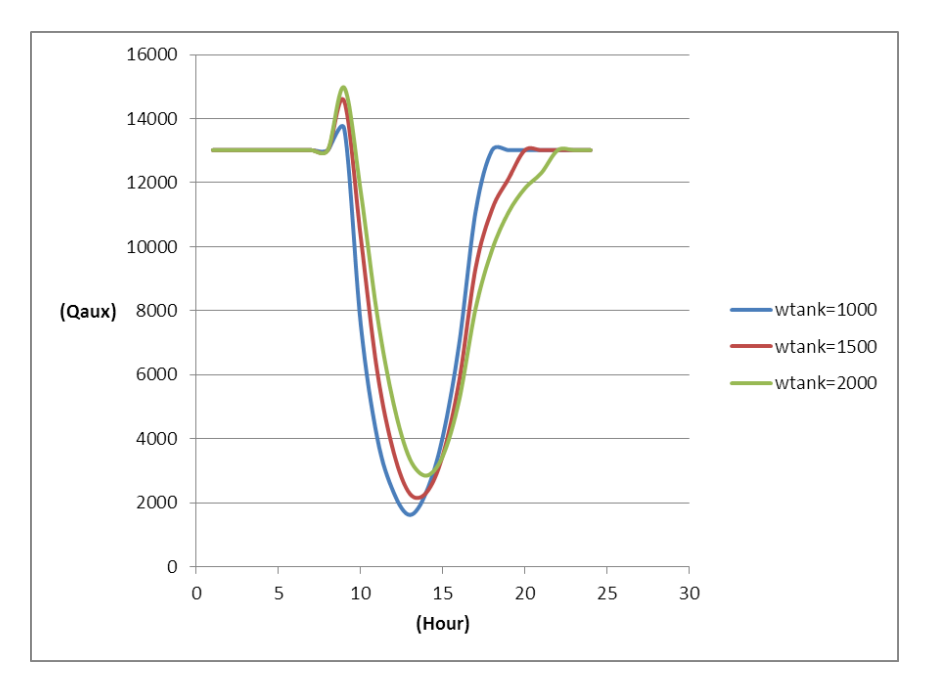


Figure 5: The change in heat load of the auxiliary heater during the day for different levels of the solar collector in May with $W_{TANK} = 1500 \text{ Kg}$, $T_{11} = 85^{\circ} C$

Thermoeconomic analysis and optimization of solar absorption refrigeration cycle

The values of mass flow rate, inlet temperature to the evaporator, efficiency, and cooling load of the system are considered nominal characteristics. Basically, the cycle itself is analyzed in order to optimally provide these values. Therefore, the mentioned parameters are not included in the decision parameters. Also, according to the analysis, the mass flow rate of the hot water entering the generator is not included in the design parameters due to not including the change in the price of the pump in the cost equations and the lack of a positive effect in reducing the price of the product.

The results of the thermoeconomic analysis of the solar absorption cycle and system sensitivity analysis

The changes in the product cost of the basic system defined in the previous sections for the change in the collector level are represented in Figure (6). The rest of the defined parameters are assumed to be constant in the basic mode. According to this figure, the product rate in the system has the lowest value at the collector level. The reason is that by increasing the area of the collector from 5 square meters to about 30 square meters and reducing the amount of fuel consumed in the auxiliary heater, a decreasing trend is observed in the product cost rate. However, with the increase in the collector level, the increase in cost due to the increase in the collector levels dominates and increases the cost rate of the product.

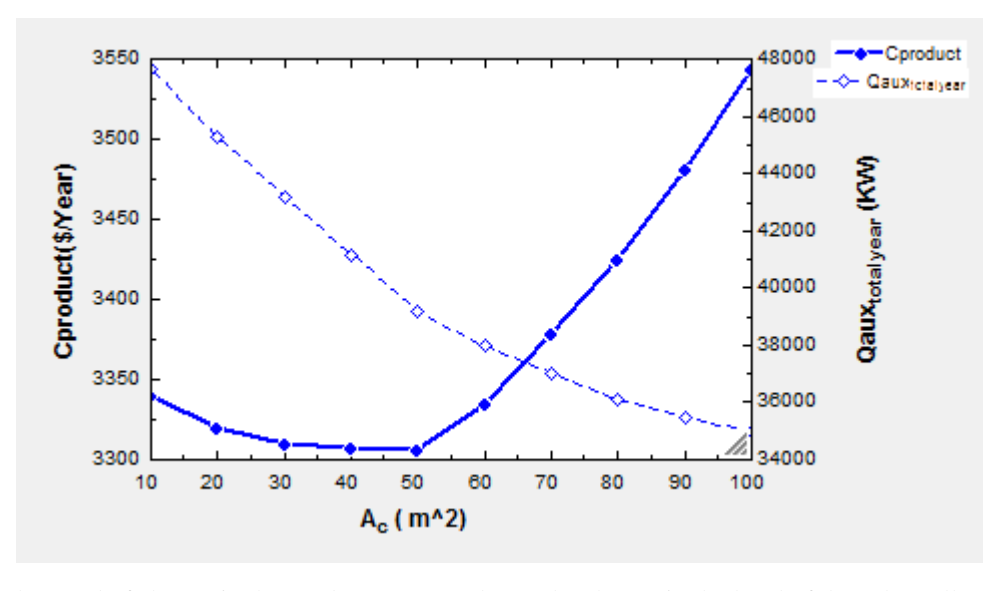


Figure 6: The trend of change in the product cost rate due to the change in the level of the solar collector

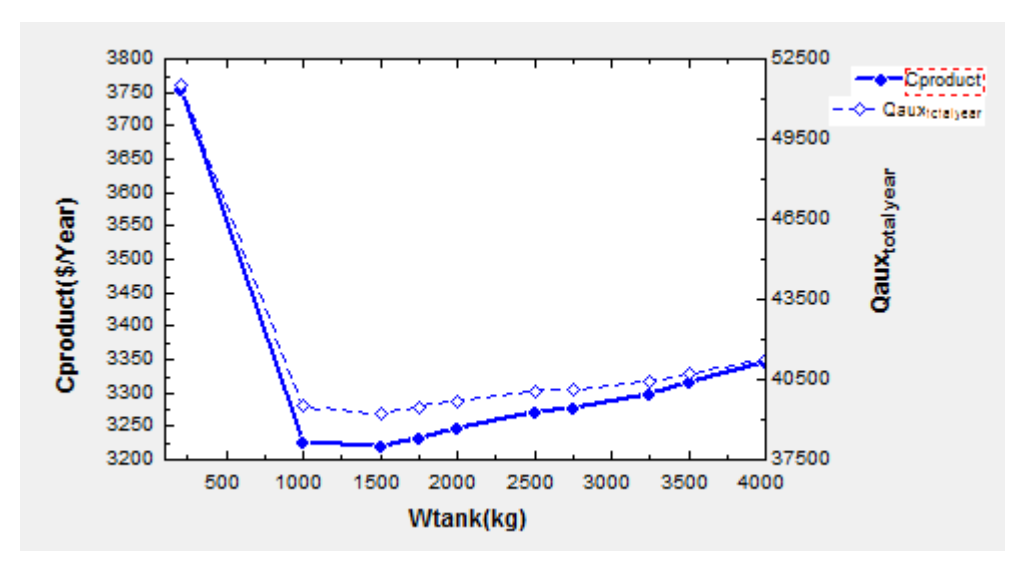


Figure 7: The change in the product cost rate due to the change in the hot water tank capacity

The trend of product cost rate changes in the evaporator relative to the change in tank capacity is represented in Figure (7). The rest of the defined parameters are assumed to be constant in the basic mode. According to the solar thermal analysis, by increasing the tank capacity due to the availability of water at high temperatures for longer hours than the operation of the system without a collector, fuel consumption in the auxiliary heater decreases, especially at the end of the day. This causes a reduction in the product cost rate in the evaporator. However, this trend is not permanent. By further increasing the capacity of the storage tank, the increase in the initial cost of the tank prevails over the reduction of the fuel cost in the auxiliary heater, as well as the effect of increasing the amount of heat consumed due to the decrease in the temperature of the tank. As a result, the cost rate of the product in the evaporator decreases.

Figure (8) represents the trend of changes in the temperature of the hot water storage tank at 14:00 in May and the annual heat consumption in the auxiliary heater relative to the change in the temperature of the hot water entering the generator.

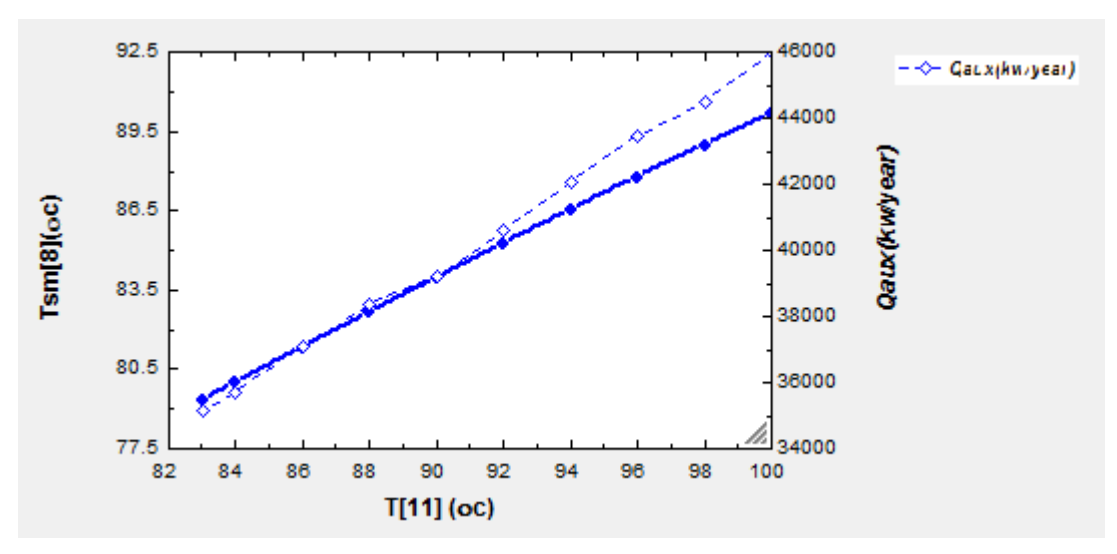


Figure 8: The trend of changes in the temperature of the hot water storage tank at 14:00 one day in May and the amount of energy consumed in the auxiliary heater compared to the changes in the temperature of the hot water entering the generator.

The rest of the parameters defined in the basic mode are assumed to be constant. As expected, the temperature of the middle node of the water in the hot water storage tank increases with the increase of the inlet temperature to the generator due to the change in the control constraints of the solar system. The amount of heat used in the heater increases slightly due to the need to use more heat to strengthen the output temperature of the heater. Figure (9) shows the change in exergy destruction and heat exchange levels in heat exchangers inside the absorption cycle. As shown in the figure, the total heat exchange levels decrease, and subsequently the total exergy losses in the

entire cycle (caused by the increase in the temperature difference of the input and output fluids in the generator, absorber, and heat exchanger on the liquid side) increase. Reducing the thermal levels in the absorption component of the cycle reduces the initial cost of the equipment and the product rate in the evaporator.

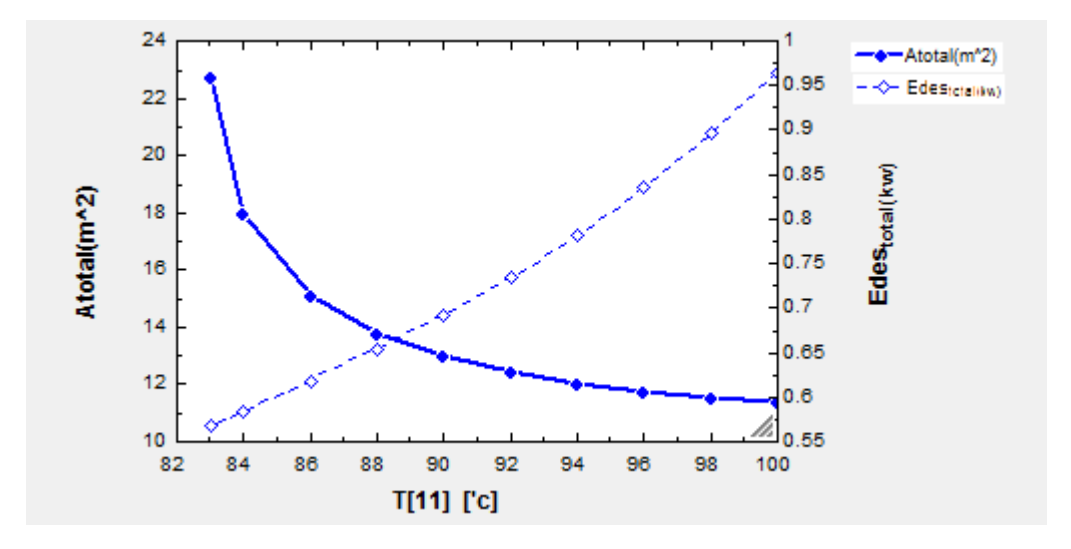


Figure 9: The trend of changes in heat exchange levels in absorption cycle equipment and exergy loss rate of the entire cycle against the change in the temperature of the hot water entering the generator

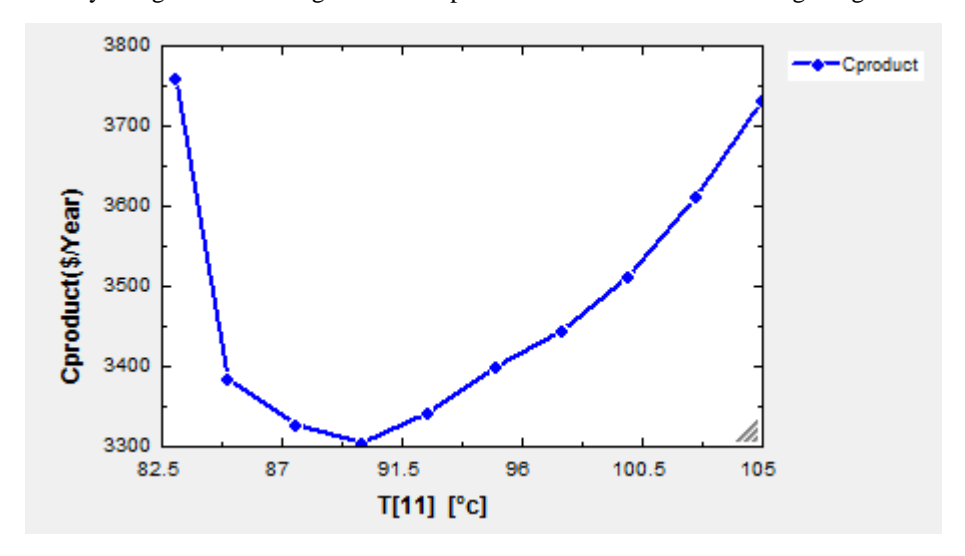


Figure 10: The trend of changes in the product production rate in the evaporator against the change in the temperature of the hot water entering the generator

According to the mentioned content, Figure (10) represents the amount of changes in the annual cost of the product in the evaporator regarding the change in the input temperature to the generator. An increase in the generator temperature leads to an increase in the product cost rate due to an increase in exergy loss costs and an increase in fuel consumption in the auxiliary heater. However, reducing the levels of heat exchangers leads to the adjustment of the product cost rate.

Figure (11) shows the changes in the heat exchange levels in the absorption component of the cycle and the exergy destruction rate caused by the effect of the change in the temperature of the cooling water entering the absorber and condenser. As shown in the figure, increasing the cooling water temperature increases the temperature of Point 1 and decreases the temperature of Point 3 (caused by the constant temperature of Point 11). In general, this causes a decrease in the temperature of the high-pressure hot water coming out of the generator and increases the fuel consumption in the auxiliary heater. The amount of exergy loss and destruction is facing an increasing trend due to the increase in temperature difference in the condenser and absorber.

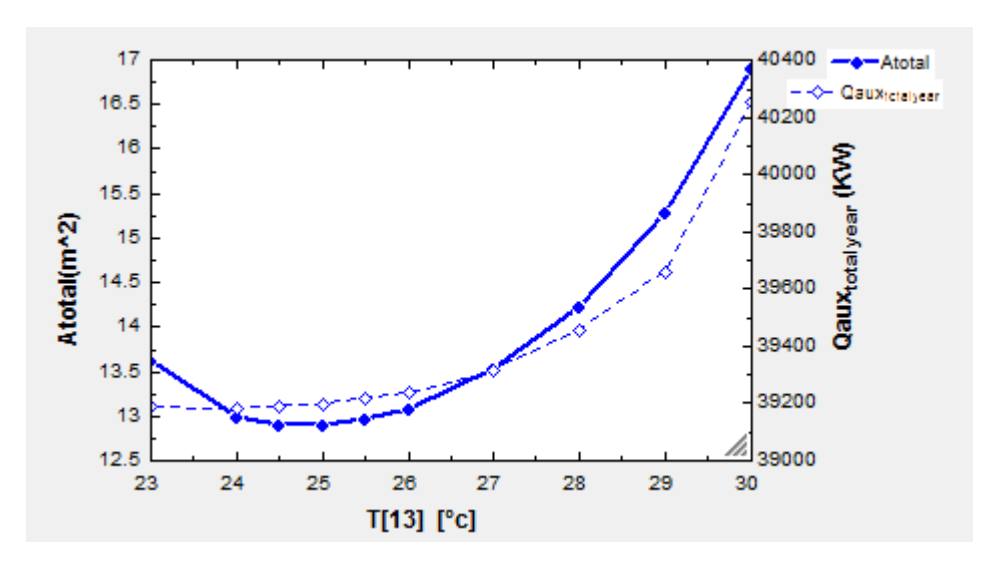


Figure 11: The trend of changes in the heat exchange levels and the amount of exergy destruction of the cycle equipment against the change in the temperature of the cooling water entering the condenser and absorber

As shown in Figure (11), first the product production rate decreases due to the dominance of the effect of reducing thermal levels. Subsequently, the product production rate increases due to the increase in efficiency and the dominance of exergy destruction effects, and the increase in the amount of fuel consumed by the generator. Therefore, at a certain point, we are faced with the minimum product production in the evaporator.

Figure (12) represents the trend of changes in exergy loss and heat exchange levels due to changes in condenser efficiency. The exergy destruction rate of the whole cycle increases due to the increase in the efficiency of the condenser and the increase in the loss of exergy in the generator and absorber, as well as the increase in the temperature difference of the incoming and outgoing flows to them. In general, this is achieved due to the change of high pressure of the cycle and the change of temperature of Point 8. As stated in the exergy analysis section, the condenser has the lowest exergetic efficiency and exergeoeconomic factor. Also, the amount of fuel consumption in the auxiliary heater increases slightly.

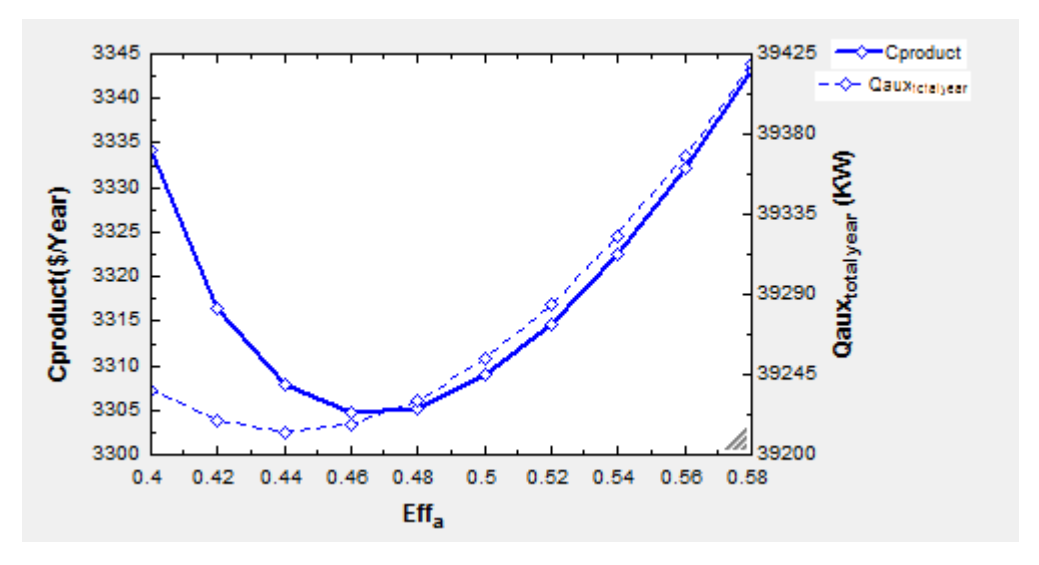


Figure 12: The trend of changes in the product production rate in the evaporator and the amount of annual heat load consumed in the auxiliary heater against the change in the efficiency of the absorber

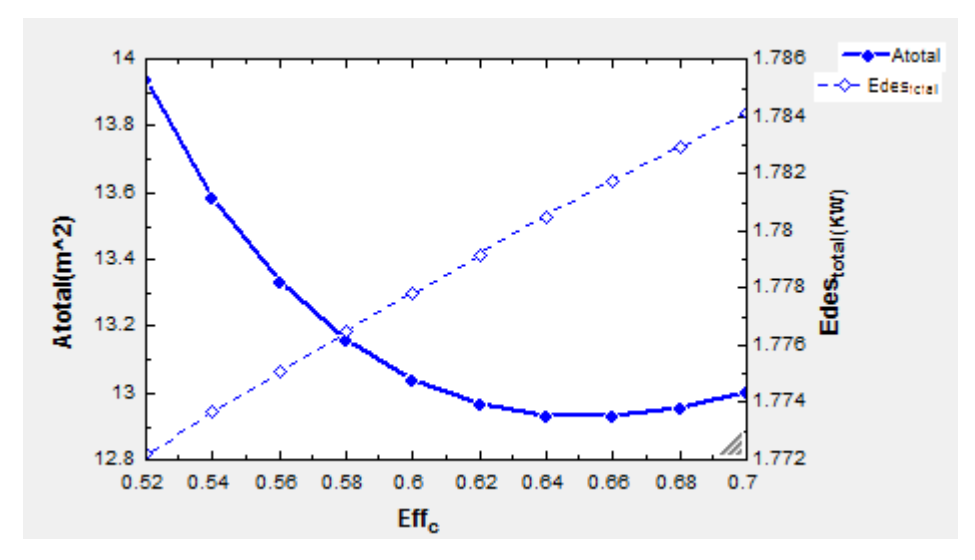


Figure 13: The trend of changes in heat exchange levels and exergy destruction rate of all cycle equipment against the change of condenser efficiency

The heat exchange levels decrease due to the increase in the temperature difference between the input and output flows to the generator and absorber. However, the level of heat exchange in the condenser increases due to the increase in the efficiency of the condenser. As shown in Figure (14), increasing the efficiency of the condenser leads to a decrease in the product production rate in the evaporator due to the dominance of the effect of reducing the capital cost in the condenser and also reducing the amount of exergy waste in the entire cycle. After that, the product production rate in the evaporator increases due to the increase in the generator and absorber levels. Therefore, at a certain point, we are faced with the minimum product production in the evaporator.

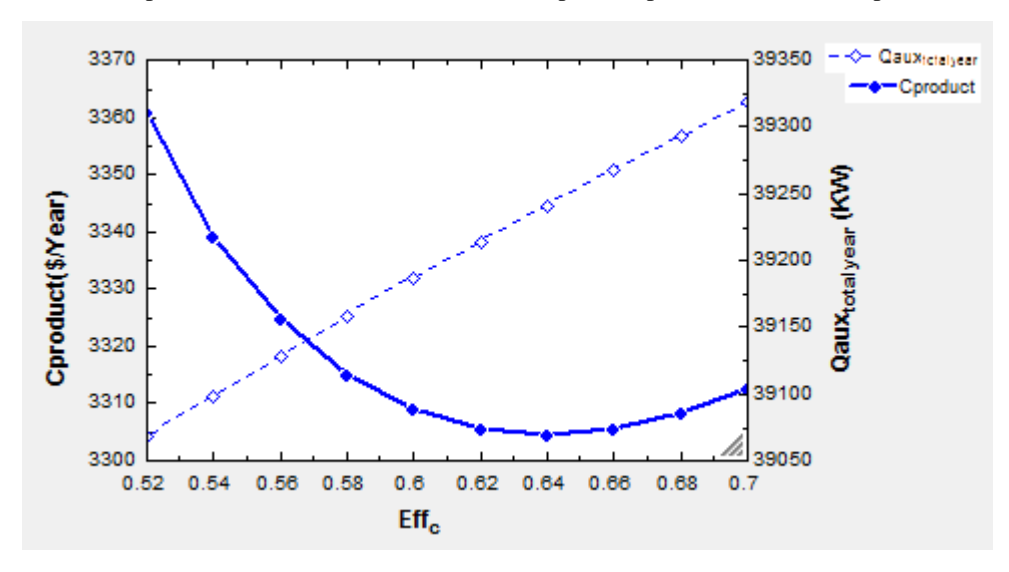


Figure 14: The trend of changes in the product production rate in the evaporator and the amount of annual heat load consumed in the auxiliary heater against the change in the efficiency of the absorber

Finally, Figure (15) shows the change in exergy loss and heat exchange levels caused by the change in the efficiency of the liquid heat exchanger. Increasing the efficiency of the liquid heat exchanger and reducing the temperature difference between the input and output flows to the generator and absorber leads to a reduction in the amount of exergy loss and destruction in the generator, absorber, and condenser, reducing the heat exchange levels of the entire cycle (the heat level of the liquid heat exchanger increases slightly and does not have a great effect on increasing the heat exchange level of the entire cycle equipment) and reducing the fuel consumption in the auxiliary heater.

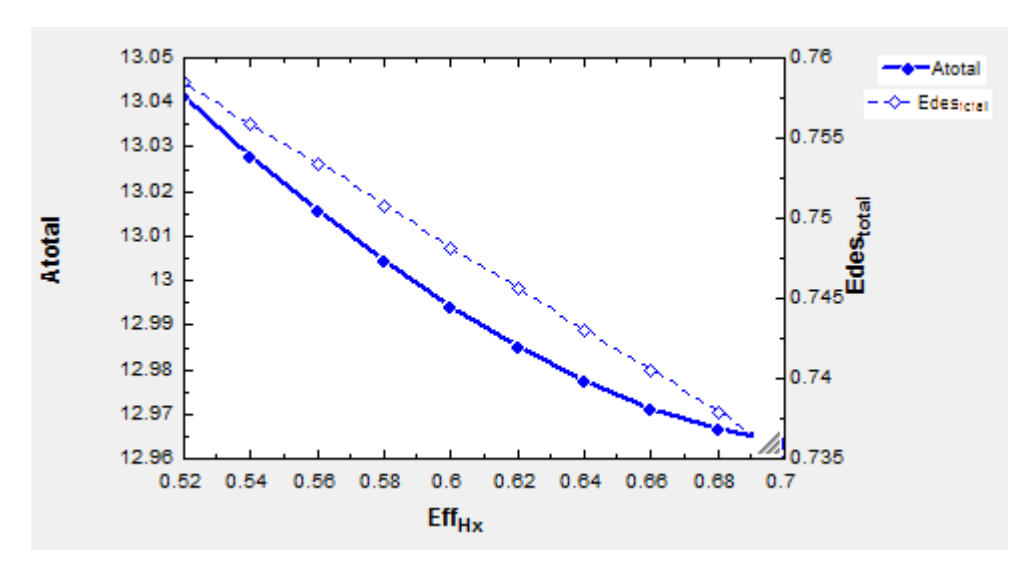


Figure 15: The trend of changes in heat exchange levels and the amount of exergy destruction of all cycle equipment against changes in the efficiency of the liquid heat exchanger

As a result, with the increase in the efficiency of the liquid heat exchanger, the trend of changing the product production rate in the evaporator is downward (Figure 16).

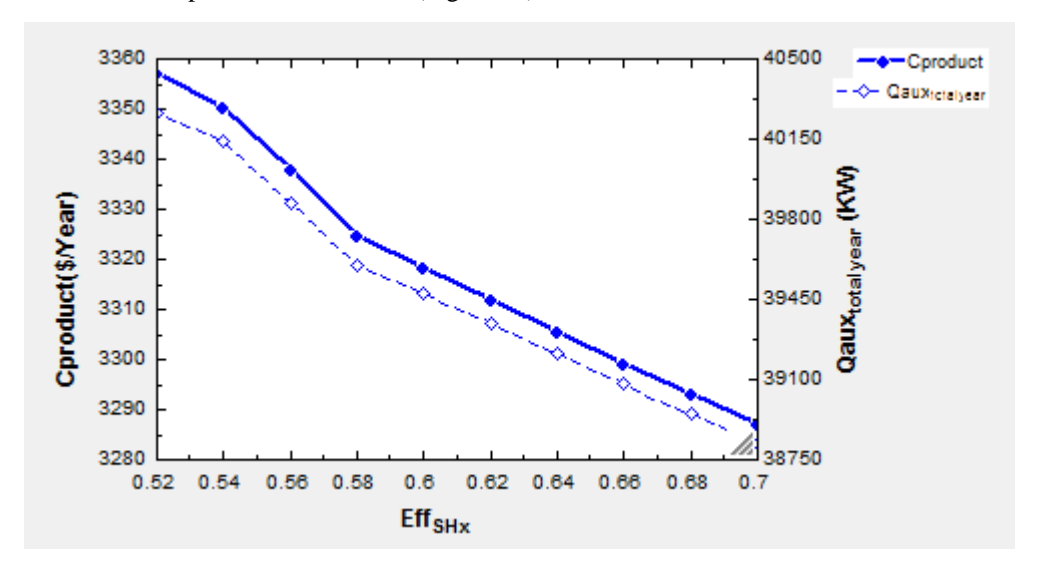


Figure 16: The trend of changes in the product production rate in the evaporator and the amount of annual heat load consumed in the auxiliary heater against the change in the efficiency of the liquid heat exchanger

Optimizing selective solar single-effect absorption refrigeration cycle

The objective function is formulated as follows:

minimize
$$C_p = \dot{C}_H + \dot{C}_E + \sum \dot{Z}_k$$
 (6)
 $83^{\circ}C < T_{11} < 100^{\circ}C$
 $25^{\circ}C < T_{13} = T_{15} < 30^{\circ}C$
 $0.55 < \varepsilon_g < 0.65$
 $0.4 < \varepsilon_a < 0.6$
 $0.5 < \varepsilon_c < 0.7$
 $0.5 < \varepsilon_{ShX} < 0.7$
 $10m^2 < A_C < 100m^2$
 $1000l < W_{Tank} < 4000l$

Table 7: Comparison of the optimal values with the basic values obtained from the thermoeconomic
optimization of the lithium bromide-water single-effect solar absorption cycle

Input variable for cycle analysis	Basic value	The optimal value
T ₁₁	90°C	87.4 °C
$T_{13} = T_{15}$	25.5℃	23 °C
$arepsilon_{ShX}$	0.64	0.7
$arepsilon_g$	0.61	0.556
ε_a	0.45	0.552
ε_c	0.62	0.7
A_C	50	43.02
W_{Tank}	1500	1042

In Table (8), the specifications and important parameters of the system in the optimal mode are presented in comparison with the basic mode. As shown in the table, the product cost rate is highly dependent on changes in hot water temperature entering the generator as well as the costs of the solar component of the system. The exergetic efficiency of the whole system is increased due to the reduction in waste and destruction of exergy. Finally, the performance coefficient of the whole system is associated with a slight increase, indicating no significant change in system efficiency.

Table 8: Optimal thermoeconomic parameters in comparison with the base case

Variance (%)	Optimal mode	Basic mode	Specification
-15.38	626.4	740.3	Capital cost of the generator, Zg(\$/Year-1)
-13.12	255.848	226.16	Absorber capital cost, Za(\$/Year-1)
-2.82	186.386	191.81	Condenser capital cost, Zc(\$/Year-1)
-0.7	41.61	41.29	Capital cost of liquid heat exchanger, Zshx(\$/Year-1)
-13.97	310.23	360.6	Collector's capital cost, Zcollector(\$/Year-1)
-30.53	62.62	90.15	Capital cost of hot water storage tank, Ztank (\$/Year-1)
-5.9	1450	1541	Total system capital cost, Ztotal (\$/Year-1)
-2.43	1722	1765	System fuel cost, CF,total(\$/Year-1)
-4.00	3172	3306	System production cost, CP,total(\$/Year-1)
-12.58	4021	4600	Exergy destruction cost of the system, CD,total(\$/Year-1)
-27.04	101.2	1087	Exergy loss cost of the system, CL,total(\$/Year-1)
6.94	17.87	16.71	System exergy efficiency (%)
3.14	0.854	0.828	System COP

IV. CONCLUSION

The process of exergy analysis was applied to the absorptive component of the system. Exergetic efficiency values and exergy loss and destruction values in the whole system were determined. The results proved that the amount of exergy destruction in the absorber and condenser is high due to the high-temperature difference between the input and output flows to the equipment. Dynamic and time-dependent thermal analysis of the system was applied 24 hours a day in the hot months of the year, taking into account the variable values of solar radiation and ambient temperature during the day. In order to obtain accurate results and correct analysis of the system, it is necessary to apply dynamic analysis to the system.

The dynamic analysis of a sample of the solar absorption refrigeration system showed that the load of the auxiliary heater (Q_{aux}) at the end of the day, at night, and at the beginning of the morning is equal to the amount of heat required in the generator. In fact, the solar system does not contribute to providing the necessary load in the generator, that is, the value of FNP is equal to zero. However, as the day begins and the hours increase towards noon, the solar system works effectively. Around 14:00 in the afternoon, the solar system provides about 90% of the necessary thermal load of the generator.

The temperature of the middle node of the tank increased during the day due to the increase in the collector level. Also, the temperature of the middle node of the tank reached its peak at noon due to the increase in the intensity of direct solar radiation to the collector levels. The increase in the tank temperature during the day due to the increase in the collector level led to a decrease in the energy consumption in the auxiliary heater to provide the required water temperature at the generator inlet.

Increasing the volume of the tank led to a decrease in the maximum temperature in the tank. However, it is evident in the upward trend of the average tank temperature during the day and night hours. This causes an increase in the volume of the hot water storage tank to reduce the energy consumption in the auxiliary heater to provide the required water temperature at the generator inlet.

After the exergetic and thermodynamic analysis and combining it with the dynamic analysis of the solar component, thermoeconomic analysis was applied to the system and the annual fuel consumption of the system and the annual rate of cooling production in the system were calculated. Subsequently, the effect of different parameters of the system on the annual fuel consumption and the annual cost of producing cooling in the evaporator were investigated.

The increase in collector levels increased the amount of solar energy absorbed in the system, which in turn reduced the fuel consumption in the auxiliary heater. Despite the reduction in the cost of fuel used in the auxiliary heater, increasing the collector levels greatly increased the initial cost of the system.

Increasing the capacity of the tank leads to the reduction of fuel consumption in the auxiliary heater, especially at the end of the day. This causes a reduction in the product cost rate in the evaporator. However, this trend is not permanent. The reason is that by increasing the volume of the storage tank, the increase in the initial cost of the tank prevails over the decrease in the fuel cost in the auxiliary heater and reduces the cost rate of the product in the evaporator.

With the increase in generator temperature, the product cost rate increases due to the increase in exergy loss costs and the increase in fuel consumption in the auxiliary heater. Also, reducing the levels of heat exchangers reduces the cost of the product.

Then, the effect of other cycle parameters on the annual fuel consumption and the annual cost of producing cooling in the evaporator were investigated. Finally, the system defined in the base mode was optimized from a thermoeconomic point of view. It was concluded that the annual rate of cooling production is highly dependent on the temperature of hot water entering the generator and the amount of solar collector levels. The costs caused by exergy waste and destruction and the exergetic efficiency of the system decreased and increased, respectively.

According to the results, paying attention to the change of heat transfer coefficients in the collector, hot water storage tank, and heat exchangers (caused by the change of temperature, levels, and design of the cycle heat exchangers) is necessary to increase the accuracy in the parametric analysis of the system. Also, multi-objective optimization, combined improvement of thermodynamic and thermoeconomic characteristics, and thermoeconomic comparison of different systems with different types of solar collectors are recommended for future works.

V. REFERENCES

- [1] Hu, Z., Zhang, Y., Liu, L., Yang, L., & He, S. (2018). A Nanostructure-Based High-Temperature Selective Absorber-Emitter Pair for a Solar Thermophotovoltaic System with Narrowband Thermal Emission. Progress In Electromagnetics Research, 162, 95-108.
- [2] Alshaer N, Bakhaider R, Elias AY, Yamany I, Alshouibi E, Elias W. Dental Misconceptions in Social Media Accounts: Youtube and Instagram Applications Among Fluoride Toxicity, Bleaching and, Waterjet. Annals of Dental Specialty. 2022;10(2-2022):19-24.

- [3] Mirghaed MT, Karamaali M, Bahadori M, Abbasi M. Identification and Prioritization Technologies and Types of Threats in Future Warfare Using Future Studies Approach. Entomology and Applied Science Letters. 2022;9(1-2022):7-19.
- [4] Niu, X., Qi, D., Wang, X., Cheng, Y., Chen, F., Li, B., & Gong, R. (2018). Improved broadband spectral selectivity of absorbers/emitters for solar thermophotovoltaics based on 2D photonic crystal heterostructures. JOSA A, 35(11), 1832-1838.
- [5] Wang, Y., Liu, H., & Zhu, J. (2019). Solar thermophotovoltaics: Progress, challenges, and opportunities. APL Materials, 7(8), 080906.
- [6] Kelsall, C. C. (2018). Cavity absorber-emitters for high-temperature solar thermophotovoltaics (Doctoral dissertation, Massachusetts Institute of Technology).
- [7] Zhou, J., Liu, Z., Liu, G., Pan, P., Liu, X., Tang, C., ... & Wang, J. (2020). Ultra-broadband solar absorbers for highericiency thermophotovoltaics. Optics Express, 28(24), 36476-36486.
- [8] Gamel, M. M. A., Lee, H. J., Rashid, W. E. S. W. A., Ker, P. J., Yau, L. K., Hannan, M. A., & Jamaludin, M. (2021). A Review on Thermophotovoltaic Cell and Its Applications in Energy Conversion: Issues and Recommendations. Materials, 14(17), 4944.
- [9] Gupta, M. C., & Bhatt, R. (2021, April). Micro/nanostructure-based selective absorber and emitter surfaces for high-efficiency solar thermophotovoltaic (STPV) applications. In Energy Harvesting and Storage: Materials, Devices, and Applications XI (Vol. 11722, p. 1172204). International Society for Optics and Photonics.
- [10] Feng, D., Yee, S. K., & Zhang, Z. M. (2021). Improved performance of a near-field thermophotovoltaic system by a back gapped reflector. arXiv preprint arXiv:2107.09772.
- [11] Polevoy GG, Sablin AB. The Influence of Burpee on the Distribution of Attention of Schoolchildren 15-16 Years Old. Archives of Pharmacy Practice. 2022;13(3-2022):29-32.
- [12] Nakagawa N, Odanaka K, Ohara H, Ito T, Kisara S, Ito K. Effect of smartphone location on pharmacy students' attention and working memory. Journal of Advanced Pharmacy Education and Research. 2022;12(2-2022):84-90.
- [13] Bierman, D. M., Lenert, A., Chan, W. R., Bhatia, B., Celanovic, I., Soljacic, M., & Wang, E. N. (2017, June). Nanoengineered devices for solar energy conversion. In 2017 19th International Conference on Solid-State Sensors, Actuators and Microsystems (TRANSDUCERS) (pp. 698-701). IEEE.
- [14] Zhou, Z., Jiang, C., Wu, H., & Zhang, B. Design and Theoretical Study of a Metamaterial Absorber-Emitter Pair Matched with a Low-Bandgap PV Cell for an STPV System. Available at SSRN 3913082.
- [15] Bhatt, R., Kravchenko, I., & Gupta, M. (2020). High-efficiency solar thermophotovoltaic system using a nanostructure-based selective emitter. Solar Energy, 197, 538-545.
- [16] Elzouka, M., & Ndao, S. (2017). Towards a near-field concentrated solar thermophotovoltaic microsystem: Part I—Modeling. Solar Energy, 141, 323-333.
- [17] Tran, V. T., Nguyen, H. Q., Kim, Y. M., Ok, G., & Lee, J. (2020). Photonic–Plasmonic Nanostructures for Solar Energy Utilization and Emerging Biosensors. Nanomaterials, 10(11), 2248.
- [18] N. Petchers . Combined Heating, Cooling & Power Handbook Technologies & Applications An Integrated Approach to Energy Resource Optimization. Inc NetLibrary 2003, Chapter 18.
- [19] Rejeb, O., Ghenai, C., & Bettayeb, M. (2020). Modeling and simulation analysis of solar absorption chiller driven by nanofluid-based parabolic trough collectors (PTC) under hot climatic conditions. Case Studies in Thermal Engineering, 19, 100624.
- [20] Xu, Z. Y., & Wang, R. Z. (2017). Simulation of solar cooling system based on variable effect LiBr-water absorption chiller. Renewable energy, 113, 907-914.
- [21] Khan, M. S. A., Badar, A. W., Talha, T., Khan, M. W., & Butt, F. S. (2018). Configuration based modeling and performance analysis of single effect solar absorption cooling system in TRNSYS. Energy Conversion and Management, 157, 351-363.
- [22] Ghaith, F. A. (2017). Performance of solar powered cooling system using Parabolic Trough Collector in UAE. Sustainable Energy Technologies and Assessments, 23, 21-32.
- [23] M. Valdes, M.D. Duran, A. Rovira, Thermoeconomic optimization of combined cycle gas turbine power plants using genetic algorithms, Appl.Therm. Eng. 23 (2003) 2169–2182, ISSN 1359-4311.